Fast, Jerome D.; Heilman, Warren E. 2003. The effect of lake temperatures and emissions on ozone exposure in the western Great Lakes region. Journal of Applied Meteorology. 42: 1197-1217.

The Effect of Lake Temperatures and Emissions on Ozone Exposure in the Western Great Lakes Region

JEROME D. FAST

Pacific Northwest National Laboratory, Richland, Washington

WARREN E. HEILMAN

North Central Research Station, USDA Forest Service, East Lansing, Michigan

(Manuscript received 8 August 2002, in final form 12 December 2002)

ABSTRACT

A meteorological–chemical model with a 12-km horizontal grid spacing was used to simulate the evolution of ozone over the western Great Lakes region during a 30-day period in the summer of 1999. Lake temperatures in the model were based on analyses derived from daily satellite measurements. The model performance was evaluated using operational surface and upper-air meteorological measurements and surface chemical measurements. Reasonable agreement between the simulations and observations was obtained. The bias (predicted − observed) over the simulation period was only −1.3 ppb for the peak ozone mixing ratio during the day and 5.5 ppb for the minimum ozone mixing ratio at night. High ozone production rates were produced over the surface of the lakes as a result of stable atmospheric conditions that trapped ozone precursors within a shallow layer during the day. In one location, an increase of 200 ppb of ozone over a 9-h period was produced by chemical production that was offset by losses of 110 ppb through vertical mixing, horizontal transport, and deposition. The predicted ozone was also sensitive to lake temperatures. A simulation with climatological lake temperatures produced ozone mixing ratios over the lakes and around the lake shores that differed from the simulation with observed lake temperatures by as much as 50 ppb, while the differences over land were usually 10 ppb or less. Through a series of sensitivity studies that varied ozone precursor emissions, it was shown that a reduction of 50% in NO_x or volatile organic compounds would lower the 60-ppb ozone exposure by up to 50 h month^{-1} in the remote forest regions over the northern Great Lakes. The implications of these results on future climate change and air quality in the region are discussed.

1. Introduction

In addition to the effects of ozone on human health (McKee 1994), it is well-known that high surface ozone concentrations can have an adverse effect on many different types of vegetation in the upper Great Lakes region. For example, Coleman et al. (1995) examined the effects of ozone exposure on various aspen (*Populus tremuloides*) clones in northern Michigan. Whole-tree photosynthesis was found to decrease in all clones in response to enhanced ozone concentrations, along with early leaf abscission. A 5-yr study by Karnosky et al. (1993) found varying degrees of sensitivity to seasonal ozone exposure on growth, physiology, and carbon allocation for three different types of tree species (*Acer saccharum*, *Pinus strobus*, and *Populus tremuloides*). Ozone was found by Tjoelker et al. (1995) to reduce net photosynthesis in light-saturated areas of the canopy and to increase dark respiration in a stand of sugar maple (*Acer saccharum*). Other studies of the effects of ozone on vegetation common in the western Great Lakes region have been performed by Wang et al. (1986), Armentano and Menges (1987), Bennett et al. (1992, 1994), Volin et al. (1993), Reich et al. (1990), and Rezabek et al. (1989).

These studies have filled a gap in our understanding of the importance of vegetation/ozone interactions, but information is also needed on the relevant photochemical processes that lead to high surface ozone episodes and the meteorological processes that transport ozone from urban areas to remote sites containing ozone-sensitive vegetation. The Lake Michigan Ozone Study (LMOS; Koerber et al. 1991) and the Program for Research on Oxidants: Photochemistry, Emissions, and Transport (PROPHET; Carroll et al. 2001) are the most recent field experiments that have collected meteorological and chemical measurements in the region.

LMOS was an air quality field campaign, conducted over a 7-week period during the summer of 1991, in which measurements were made by surface monitoring

Corresponding author address: Jerome Fast, Pacific Northwest National Laboratory, P.O. Box 999, K9-30, 3200 Q Avenue, Richland, WA 99352.
E-mail: jerome.fast@pnl.gov

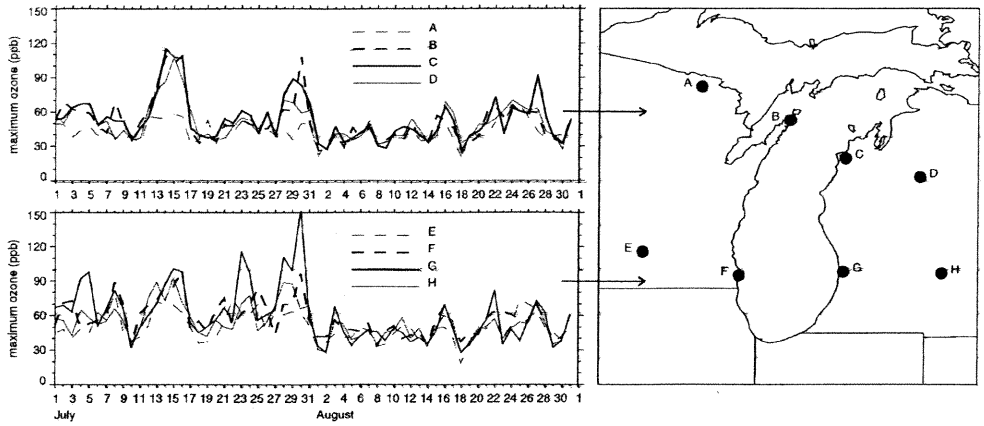

FIG. 1. Time series of daily maximum ozone in the vicinity of Lake Michigan at eight ozone monitoring stations during Jul and Aug of 1999.

stations, aircraft, and boats. An analysis of the observations by Dye et al. (1995) revealed that the highest ozone concentrations occurred in a shallow cool layer adjacent to Lake Michigan and were subsequently transported to the shores of Wisconsin and Michigan. Sillman et al. (1993) showed that suppressed vertical mixing and deposition in a model were needed to produce high ozone concentrations over the lake. Several mesoscale modeling studies have been performed to evaluate their ability to simulate lake-breeze circulations (Eastman et al. 1995) and to assess how local circulations could influence ozone transport (Lyons et al. 1995; Hanna and Yang 2001; Shafran et al. 2000). Similar to previous studies of the eastern United States (e.g., Vukovich 1979 and others), meteorological analyses by Hanna and Chang (1995) and Dye et al. (1995) showed that high-ozone events in the region resulted from local sources contributing to an already polluted air mass associated with a high pressure system. Hanna et al. (1996) found that U.S. Environmental Protection Agency (EPA) regulatory models underpredicted ozone and ozone precursors 200–500-km downwind of the major sources, where ozone concentrations greater than 150 ppb were observed.

In contrast with most air quality field campaigns that collect extensive data over a wide area for a short period of time, PROPHET has collected extensive chemical measurements at a single remote site in northern Michigan over the past several years. While PROPHET has focused on the photochemical processes within and just above the forest canopy at this rural site, it also has assessed the role of transport processes and the impact of upwind anthropogenic and biogenic emissions in the Midwest. For example, meteorological analyses and back trajectories indicated that changes in the local chemistry could be explained by rapid and frequent transitions between clean Canadian air and regions of higher anthropogenic emissions in the United States (Cooper et al. 2001).

In this study, we employ a coupled meteorological and chemical model to simulate the evolution of ozone in the western Great Lakes region over a 30-day period. Because the lakes compose a large fraction of the surface area of the region, the effect of lake temperatures on the production of ozone will be quantified. To examine how ozone concentrations and ozone exposure are affected by local pollutant sources, a series of sensitivity simulations are performed that vary ozone precursor emission rates. This study is also intended to be a first step toward determining future ozone exposure patterns resulting from regional-scale landscape change predictions; therefore, the implications of the findings on factors needed to be accounted for by climate chemistry models will be discussed.

2. Model description and experimental design

A coupled meteorological and chemical modeling system is employed to simulate the production/destruction, turbulent mixing, transport, and deposition of ozone over the western Great Lakes region. A 30-day period between 15 July and 14 August 1999 was simulated. This period was chosen because there were days with both high and low ozone concentrations over the Great Lakes region, as shown in Fig. 1. This allowed for the investigation of the effects of emission rates and lake temperatures on ozone concentrations for a variety of meteorological conditions. Climatological studies have shown that high-ozone episodes in the eastern United States often occur along the back sides of slow-moving, persistent Bermuda high pressure systems (e.g., Vukovich 1995). During July of 1999, there were several periods in which the meteorological conditions were conducive to local ozone production and regional-scale ozone transport into the Great Lakes region. After 1 August, however, the daily peak ozone mixing ratios were lower because the region was under the influence of a series of continental high pressure systems.

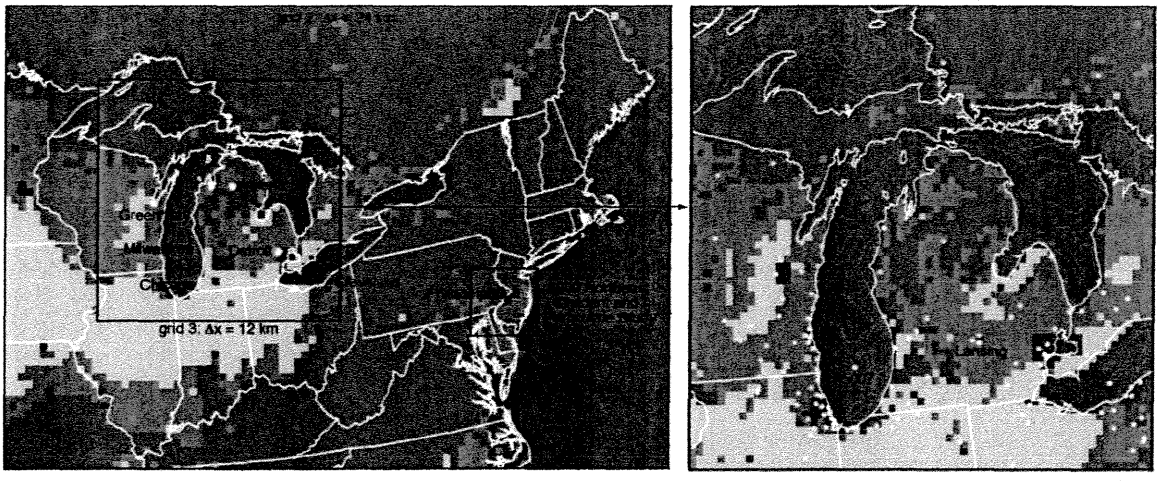

FIG. 2. Dominant vegetation types with the [(a): left panel] second and [(b): right panel] third modeling domains: crop (light green), grass (medium green), forest (dark green), and urban (red). NWS rawinsonde stations (yellow dots) in the western Great Lakes region are shown in (a) and EPA ozone monitoring stations are shown in (b). In (b), surface lake temperatures (red contours) on 15 Jul 1999 and the locations of meteorological stations (white dots) described in the text are shown.

The Northeast Oxidant and Particulate Study (NE-OPS) field campaign (Philbrick et al. 2002) took place during this 30-day period so that additional surface and upper-air meteorological and chemical measurements could be used to evaluate results in a portion of the modeling domain. While the NE-OPS field campaign took place in the vicinity of Philadelphia, Pennsylvania, downwind of the Great Lakes region, the chemistry data aloft provide critical information needed to evaluate how well the model simulates regional-scale transport of pollutants from upwind sources. A complete description of the model, the Pacific Northwest National Laboratory (PNNL) Eulerian Gas and Aerosol Scalable Unified System (PEGASUS), and its application to the NE-OPS field campaign is given in Fast et al. (2002); therefore, we briefly describe next only the details relevant to the present study.

a. Meteorological model

Version 4.3 of the Regional Atmospheric Modeling System (RAMS) mesoscale model (Pielke et al. 1992) was used to simulate the meteorological conditions between 1200 UTC 15 July and 1200 UTC 14 August. RAMS employs a two-way interactive nested grid structure, and in this study the model domain consisted of three domains. The first domain included most of eastern North America, with a grid spacing of 48 km. The second domain, shown in Fig. 2, encompassed the north-central and northeastern United States and southern Canada, with a 24-km grid spacing, while the third domain encompassed the western Great Lakes, with a 12-km grid spacing. A terrain-following coordinate system was used with a vertical grid spacing of 25 m adjacent to the surface, which gradually increased to 600 m near the model top at 20 km. Because of the staggered vertical coordinate, the first grid point was 12.5 m AGL.

The turbulence parameterization consists of a simplified second-order closure method that employs a prognostic turbulence kinetic energy equation (Mellor and Yamada 1982; Helfand and Labraga 1988). A cumulus parameterization was activated to produce cloud water and precipitation. The shortwave and longwave parameterizations include cloud effects to determine the heating or cooling caused by radiative flux divergences. Prognostic soil–vegetation relationships were used to calculate the diurnal variations of temperature and moisture at the ground–atmosphere interface. The distribution of the dominant vegetation categories (crop, grass, forest, and urban) is shown in Fig. 2. Soil moisture was initialized using values obtained from the National Centers for Environmental Prediction's Aviation (AVN) Model. Turbulent sensible heat, latent heat, and momentum fluxes in the surface layer were calculated from similarity equations. Lake temperatures in the model varied linearly in time, based on the National Oceanic and Atmospheric Administration's (NOAA) Great Lakes Environmental Research Laboratory (GLERL) daily analyses derived from satellite data. The analyses, which employ a horizontal grid spacing of about 3 km, were averaged to the 12-km grid, and the initial values on 15 July 1999 are shown in Fig. 2b.

Application of a four-dimensional data assimilation (4DDA) technique (Fast 1995) was necessary to limit the forecast errors in the meteorological fields over the long simulation period. In this study, 4DDA nudged the horizontal u and v components of the wind, potential temperature, and humidity into closer agreement with the 6-h analyses from the AVN model. A relaxation coefficient of 4.6×10^{-5} s^{-1} was used. While the stan-

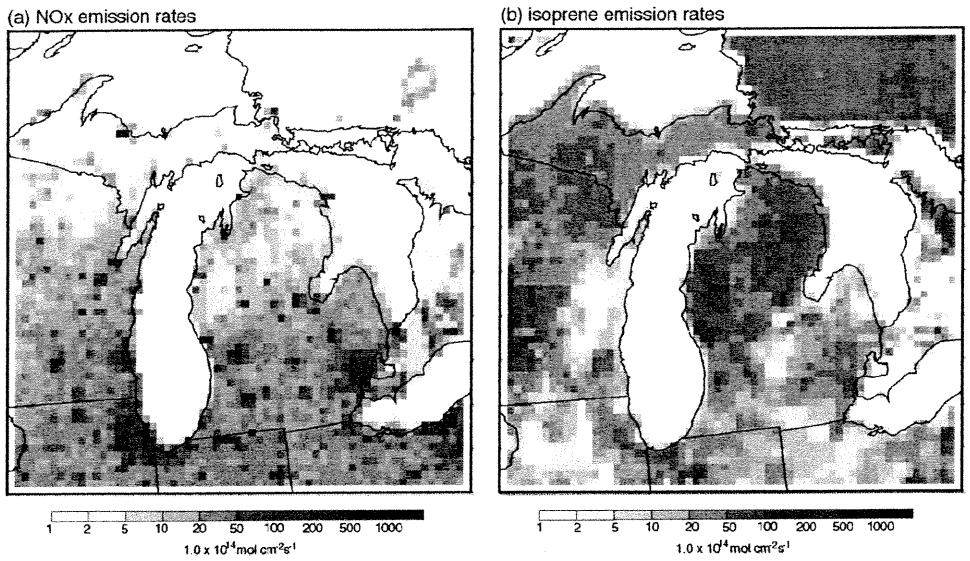

FIG. 3. Emissions of (a) NO_x and (b) isoprene on grid 3 at 1800 UTC 15 Jul 1999.

dard upper-air soundings at 0000 and 1200 UTC, such as the soundings at Green Bay, Wisconsin, and Alpena and Detroit, Michigan, shown in Fig. 2, are not included directly by 4DDA, they are included indirectly through the large-scale analyses.

b. Chemical transport model

The Eulerian chemical transport model includes emission, transport, vertical diffusion, chemical production/destruction, and dry deposition terms. The gas-phase chemistry in PEGASUS is modeled with the Carbon Bond Mechanism (CBM)-Z (Zaveri and Peters 1999) that contains 53 species and 133 reactions. CBM-Z employs the lumped-structure approach for condensing organic species and reactions, and is based on the widely used version IV (CBM-IV) developed by Gery et al. (1989) for use in urban airshed models.

The domain for the chemical model coincided with the RAMS nested grids shown in Fig. 2. While the meteorological grid extended up to 20 km AGL, chemistry was simulated up to 6 km AGL. Hourly meteorological fields (horizontal and vertical wind components, temperature, humidity, eddy diffusivity, fractional area cloud coverage, and surface properties) were obtained from the mesoscale model. The initial and lateral boundary conditions for the Great Lakes domain (Fig. 2b) were obtained from grid 2 (Fig. 2a). For grid 2, the initial, lateral, and top boundary conditions for ozone were based on climatological and observed ozonesonde profiles. The initial conditions for the other trace gas species on grid 2 were assigned low background values and were held constant during the simulation period. The associated mixing of trace gases with the large-scale cloud fields was reflected in modifications to the vertical velocity and turbulent kinetic energy (and, thus, eddy diffusivity) fields. Thus, large-scale cloud mixing was included, but subgrid cloud mixing (e.g., fair weather cumulus) was not. Photolysis rates were modified by clouds, similar to Chang (1987), using the fractional area cloud coverage.

Hourly emission rates of 14 species were obtained from the Sparse Matrix Operator Kernel Emissions (SMOKE) model (Houyoux et al. 2000). For this study, the emissions were based on the meteorological conditions from the RAMS simulation that varied hourly over the 30-day period. The SMOKE emissions were generated offline on a 4-km grid over the eastern United States and Canada, using RAMS meteorological values interpolated to the 4-km grid. The emissions were then aggregated to the 12-km grid spacing used by the PEGASUS simulation. The NO_x [sum of nitric oxide (NO) and nitrogen dioxide (NO_2)] and isoprene emissions at 1800 UTC 15 July, a Thursday, are shown in Fig. 3 to illustrate the spatial distribution over the Great Lakes modeling domain. Emissions were vertically resolved by SMOKE for the lowest eight layers of PEGASUS. Emissions above the first layer are primarily from point sources, such as those from power plant stacks. The highest NO_x emission rates occurred over urban areas. A few point sources with high emission rates are located in rural areas along the shores of Lake Superior and Lake Huron. The highest isoprene emission rates occurred in Canada, northern Michigan, and northern Wisconsin, where forest vegetation types dominate (Fig. 2b), while low isoprene emission occurred over crop areas.

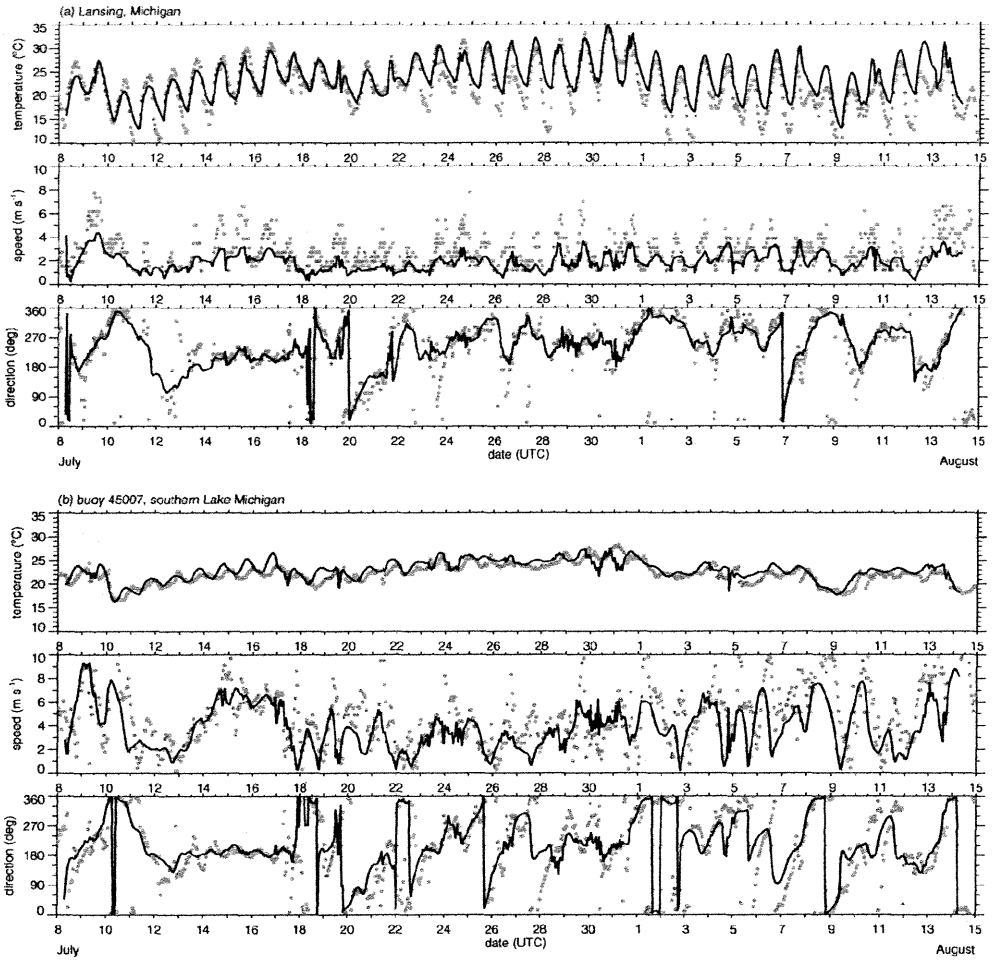

FIG. 4. Time series of observed (dots) and simulated (lines) temperature, wind speed, and wind direction for (a) Lansing, MI, and (b) moored buoy 45007.

3. Results

We first present a comparison of the observed and simulated meteorological and chemical values during the 30-day period. The model run described in the previous section is referred to as the *control simulation.* The results of a series of sensitivity simulations are then presented in section 4 to examine the effect of lake temperature and emission rates on ozone exposure in the region.

a. Boundary layer properties

The simulated meteorological fields were compared with surface observations over the model domain and profiles of wind, temperature, and humidity from the standard rawinsonde profiles at 0000 and 1200 UTC. An example of the observed and predicted surface quantities for Lansing, Michigan and buoy 45007, located in southern Lake Michigan (Fig. 2b), is shown in Fig. 4. For Lansing (Fig. 4a), the model reproduced the magnitude and multiday variation of the maximum surface temperature well. The simulated nighttime minimum temperatures were usually 1°–3°C too high after 23 July, except for a few nights that were 3°–9°C too high. This warm nighttime bias is probably due to vertical resolution in the model. Because the first grid point was 12.5 m AGL and the observations were at 2 m AGL, strong stratification within the nocturnal boundary layer would not be adequately represented by the model. For example, a preliminary simulation with a 50-m vertical grid spacing at the surface produced nighttime temperatures higher than those shown in Fig. 4a. The predicted wind speeds and directions were similar to the observations, except that the simulated peak wind speeds during the afternoon were too low on most days.

Over the lake (Fig. 4b), the diurnal variation in tem-

TABLE 1. Bias and correlation coefficient for the hourly temperature, wind speed, and wind direction over the 30-day simulation period at the two surface stations shown in Fig. 4. All the biases are statistically significant using a Student's t test with $\alpha = 0.05$.

	Bias (model − observed)			Correlation coefficient		
	Temperaure (°C)	Speed (m s^{-1})	Direction (°)	Temperature (°C)	Speed (m s^{-1})	Direction (°)
Lansing	1.91	−0.76	−4.47	0.83	0.69	0.79
Buoy 45007	0.70	−1.00	2.30	0.78	0.52	0.82

perature was much less than over land, and the simulated temperatures were close to the observed. This was not surprising because the lower boundary condition in the model employs the observed temperature distribution derived from satellite data. The simulated diurnal variation in temperature, however, was out of phase with the observations, especially between 15 and 19 July. This may be partly due to satellite measurements that were not necessarily made at the same time each day and the linear interpolation of the lake temperatures from day to day. The performance of the model in simulating the winds over the lake was similar to Lansing (Fig. 4a), except that the model did not capture as much of the wind direction variance during the period. Significantly higher wind speeds were produced over the lake because of the smaller roughness, but, as with land stations, the peak wind speeds in the afternoon were underpredicted.

Statistics that quantify the overall errors associated with the simulated surface temperature, wind speed, and direction shown in Fig. 4 are given in Table 1. While the magnitudes of the biases over land and water were somewhat different, the temperatures at night were too high, wind speeds were too low, and wind directions were too westerly for both areas. The correlation coefficients for temperature and wind direction were between 0.78 and 0.83, indicating that the model produced much of the observed variance during the 30-day period. However, the lower correlation coefficients for wind speed were largely due to predicted peak wind speeds that were too low, as indicated by the time series in Fig. 4. The model performance at other sites located within the inner grid was similar to the values in Table 1.

A number of factors may contribute to the underprediction of the peak wind speeds. For example, the current vertical grid spacing may not be adequate to resolve strong near-surface vertical wind shears. Roughness lengths employed by the surface parameterization may be too large as well. Over the lake, the differences in the observed and simulated winds, such as those in Fig. 4b, will produce pollutant-transport errors because the shallow stable layer is decoupled from the air aloft most of the day. Over land, differences between the observed and simulated wind, such as those in Fig. 4a, become less of a factor because wind speed errors aloft were small and regional-scale transport of pollutants occurs in a deep layer during the daytime convective boundary layer.

The winds aloft were evaluated by comparing the simulated results with the 0000 and 1200 UTC rawinsonde winds that were not directly employed by 4DDA. A time series of wind speed, direction, temperature, and relative humidity at the Alpena site (Fig. 2a) at about 770 m AGL is given in Fig. 5. This level was chosen because it was usually located in the middle of the afternoon convective boundary layer. Observed winds at 770 m AGL were available at each time period, but temperature and humidity were obtained by vertical interpolation from the observed profile. Because the model employed 4DDA, the meteorological fields followed the synoptic patterns during the 30-day period and the model predicted well the observed trends in temperature, humidity, speed, and direction throughout the 30-day period. On a few days, relatively large differences occurred in the relative humidity, but there was no significant bias overall. The wind directions at Alpena and other nearby upper-air sites during the period were usually westerly or northwesterly, indicating that transport from high-pollutant sources to the south over the Ohio River valley did not occur frequently.

The bias, simulated − observed, in the wind speed, direction, temperature, and relative humidity within 3.5 km of the ground at Alpena is shown in Fig. 6. On average, the model winds were slightly lower than observed between 0.2 and 1.5 km AGL and above 3 km AGL. Somewhat larger errors between 1 and 2 m s^{-1} were produced between 1.5 and 3 km AGL. At the surface, wind speeds were 1.5 m s^{-1} too low on average, consistent with the comparison with the surface observations (Fig. 4). While there was very little bias in the wind directions near the surface and above 2.5 km AGL, the simulated directions were usually 5°–10° different than observed between 0.5 and 2 km AGL. Figure 5 indicates that some of the variance in Fig. 6 was associated with timing errors of a few hours or less. The overall errors for the other rawinsonde stations were similar to those shown in Fig. 6.

The parameters with the largest uncertainty in mesoscale models are usually associated with clouds. A qualitative agreement was found between the simulated spatial cloud distribution and satellite images of the observed cloud distribution throughout the 30-day period (not shown), especially when fronts were moving through the region. However, the amount of cloudiness was significantly different than that observed on some days at specific locations as expected.

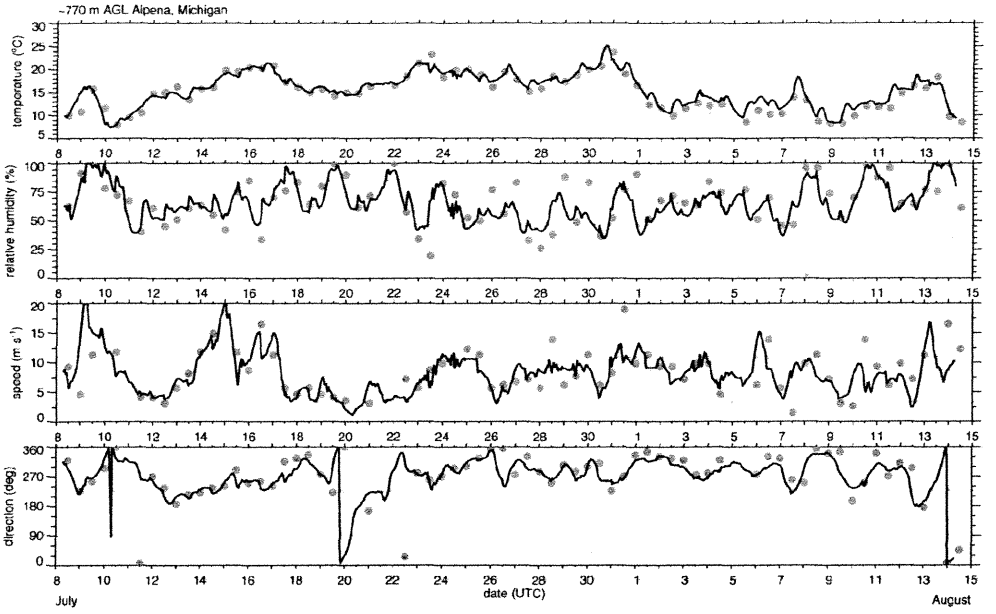

FIG. 5. Time series of observed (dots) and simulated (lines) temperature, relative humidity, wind speed, and wind direction at about 770 m AGL at Alpena, MI.

b. Air chemistry

Because the mesoscale model reproduced the main features of the observed winds and boundary layer evolution, the chemical transport model is expected to provide a reasonable estimate of regional-scale transport of pollutants over the domain shown in Fig. 2 during the 30-day period. The meteorological fields in the chemical transport model were varied linearly in time with a 5-min time step, using the archived hourly output from the mesoscale model. As discussed in section 2, the emissions that depended on the simulated meteorological fields were updated hourly.

Because of the variable surface properties in the Great Lake region (land/lake, vegetation, trace gas emission rates), a complex spatial distribution of ozone is expected. To determine how the model performance varied over the domain, 16 geographical regions denoted by the boxes shown in Fig. 7 were defined. These regions encompass portions of the lake shore or inland areas and are also based on the proximity of an ozone-monitoring station to an urban area. For example, regions 5, 13, and 16 include stations in the vicinity of Chicago, Illinois, Detroit, and Cleveland, Ohio, respectively. In remote northern areas, a small geographic region surrounding a single monitoring station is used. Simulated values from grid cells located entirely over water are excluded.

A direct comparison of the observed and simulated surface ozone over the 30-day period is shown in Fig. 8 for regions 2, 6, 7, and 10. In region 2, over northeastern Wisconsin, the model reproduced the observed evolution of ozone throughout the period. The average maximum and minimum values were usually close to observed, and the range of simulated values encompassed the range of observed values. In region 6 around Sault Ste. Marie, Michigan, the multiday trend in ozone was similar to the observed, but the average simulated maximum and minimum values were somewhat too high. The range of values, however, indicates that there were some grid cells with ozone mixing ratios similar to observations. In region 7, over northern Michigan, the range of values predicted by the model usually included the observations, but the diurnal variation was lower than observed because the minimum values were overestimated. Over central Michigan in region 10, both the average maximum and minimum simulated values were quite good, with the exception of a few days (e.g., 26 July).

The minimum values were usually predicted better in regions 2 and 10, presumably because of NO titration at night with the relatively higher emission rates in these areas. The NO emission rates in rural areas, such as regions 6 and 7, may be too low. Another factor for the positive bias in the minimum ozone values in rural areas may be that the mesoscale model produced too much mixing adjacent to the ground during the stable conditions at night. Because the emission rates were low, a slight overestimation in the vertical eddy diffusivity coefficient would be sufficient to dilute NO near the ground.

The modeling system was able to capture the spatial variations in ozone on both sides of Lake Michigan,

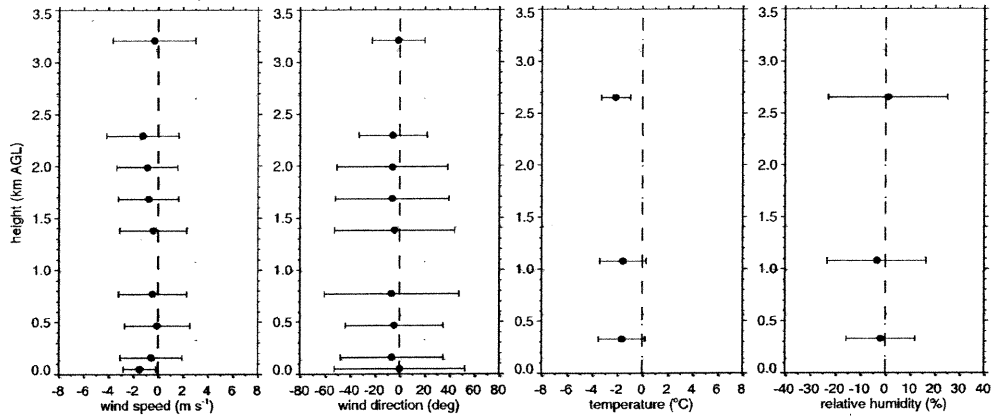

FIG. 6. Mean (dots) and 1 standard deviation (lines) of the bias in the wind speed, direction, temperature, and relative humidity at Alpena, MI, during the 30-day simulation period.

such as those depicted in Fig. 1. High-ozone concentrations were often produced over the lake and transported to the north. For example, ozone produced from precursors emitted from Chicago and Milwaukee, Wisconsin, was advected to the north during the episodes on 29 and 30 July. This northward transport was responsible for ozone mixing ratios approaching 120 ppb in northeastern Wisconsin and 70 ppb in Sault Ste. Marie (Fig. 8).

The only measurements over water are made on a ferry that travels across central Lake Michigan twice a day between Manitowoc, Wisconsin, and Ludington, Michigan, as shown in Fig. 9. Hourly averaged values from the ferry are reported so that only three points over the lake are available for each transect. The model results were averaged over the western, middle, and eastern regions of the lake (Fig. 9) and compared with the observations within those regions. The time series of the observed and simulated values indicate that the model produced a temporal and spatial variation that was consistent with the observations on most days. In general, higher ozone mixing ratios were observed and predicted over the middle and eastern portions of the lake between 23 and 31 July. The largest differences between the observed and simulated values occurred on 30 July when 130 ppb were observed while the model predicted 75 ppb, and on 31 July when 60 ppb were observed while the model predicted 120 ppb. Because there were only two observations in each region of the lake each day, not all of the temporal variability can be evaluated.

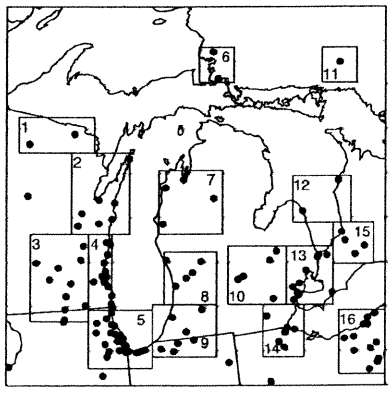

FIG. 7. The 16 geographical regions (boxes) that are used to determine how the model performance varied over the domain, and ozone monitoring stations (dots).

To illustrate some of the meteorological processes affecting ozone, an example of the ozone distribution on the afternoon of 24 July is shown in Fig. 10. At 2100 UTC (Fig. 10a), the simulated spatial ozone distribution is similar to the observed distribution. High ozone mixing ratios were predicted over the surface of each lake. The highest mixing ratios occurred over southern Lake Michigan just downwind of Milwaukee and Chicago. High ozone mixing ratios were predicted along the eastern shore of Lake Michigan, while lower mixing ratios were predicted along the western shore that were similar to the ozone monitor observations along the lake. However, the predicted ozone mixing ratios a few kilometers inland over northern Indiana and western Michigan were too low. A similar pattern was produced over Lake Huron, although there are few observations in that area. Animation of the simulated meteorological and chemical fields indicated that the high ozone mixing ratios greater than 90 ppb over eastern Lake Superior were produced by emissions from the large point source located on the southern shore (Fig. 3a). The vertical cross section shows that the high ozone mixing ratios over Lake Michigan were confined to a shallow layer within 200 m of the lake. The westerly winds advected this ozone over the eastern shore of Lake Michigan, but mixing within the deep CBL then significantly diluted the concentration of ozone over land.

The predicted evolution of ozone over Lake Michigan

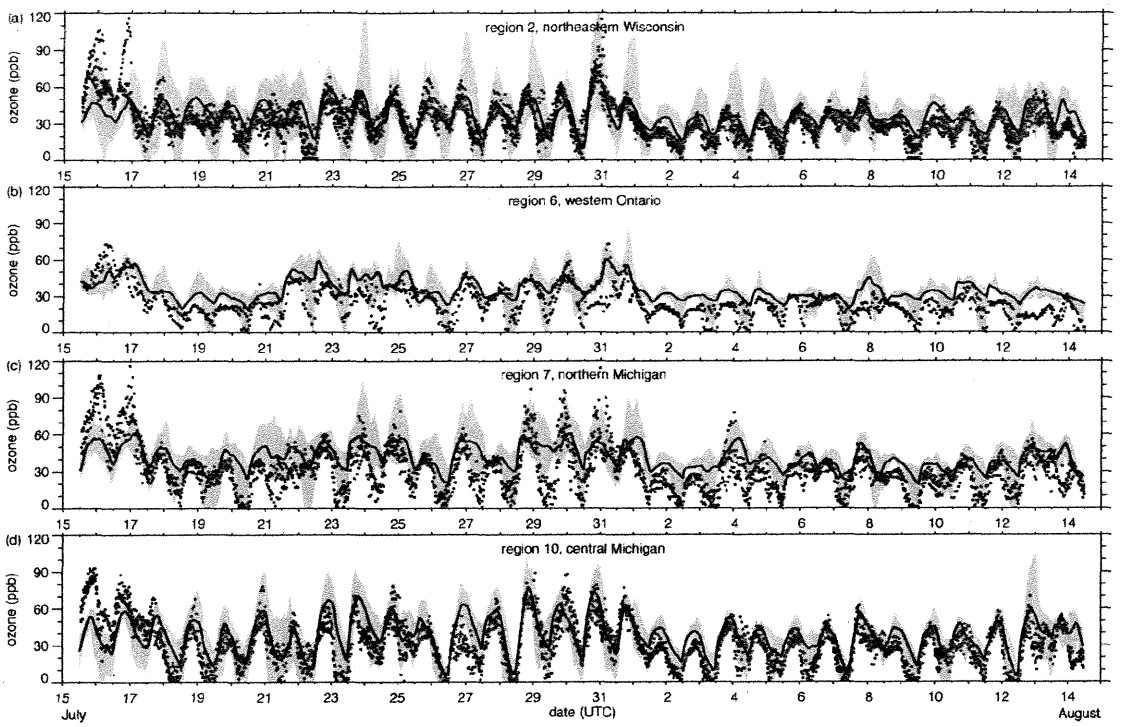

FIG. 8. Time series of observed and predicted ozone for regions (a) 2, (b) 6, (c) 7, and (d) 10: hourly observations (dots), simulated average (line), and simulated range (gray shading) within each region.

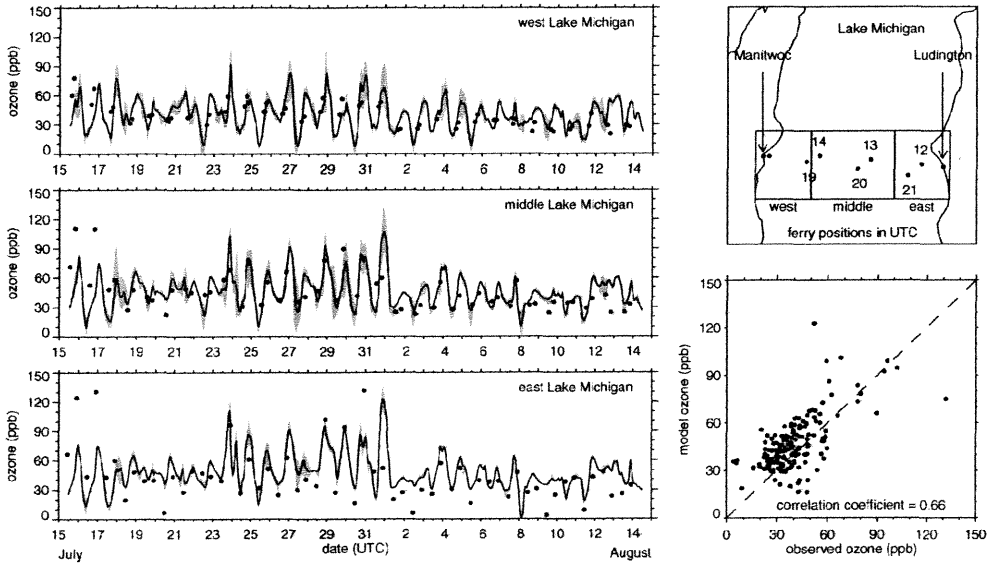

FIG. 9. Observed hourly average ozone mixing ratios obtained from measurements made on a ferry over Lake Michigan (dots) and simulated ozone (line) along the ferry transects. Observed and simulated values are averaged over western, middle, and eastern regions (boxes in the upper-right panel) and the simulated range of ozone within the boxes (gray shading). The observed vs simulated ozone for all locations is shown in the lower-right panel.

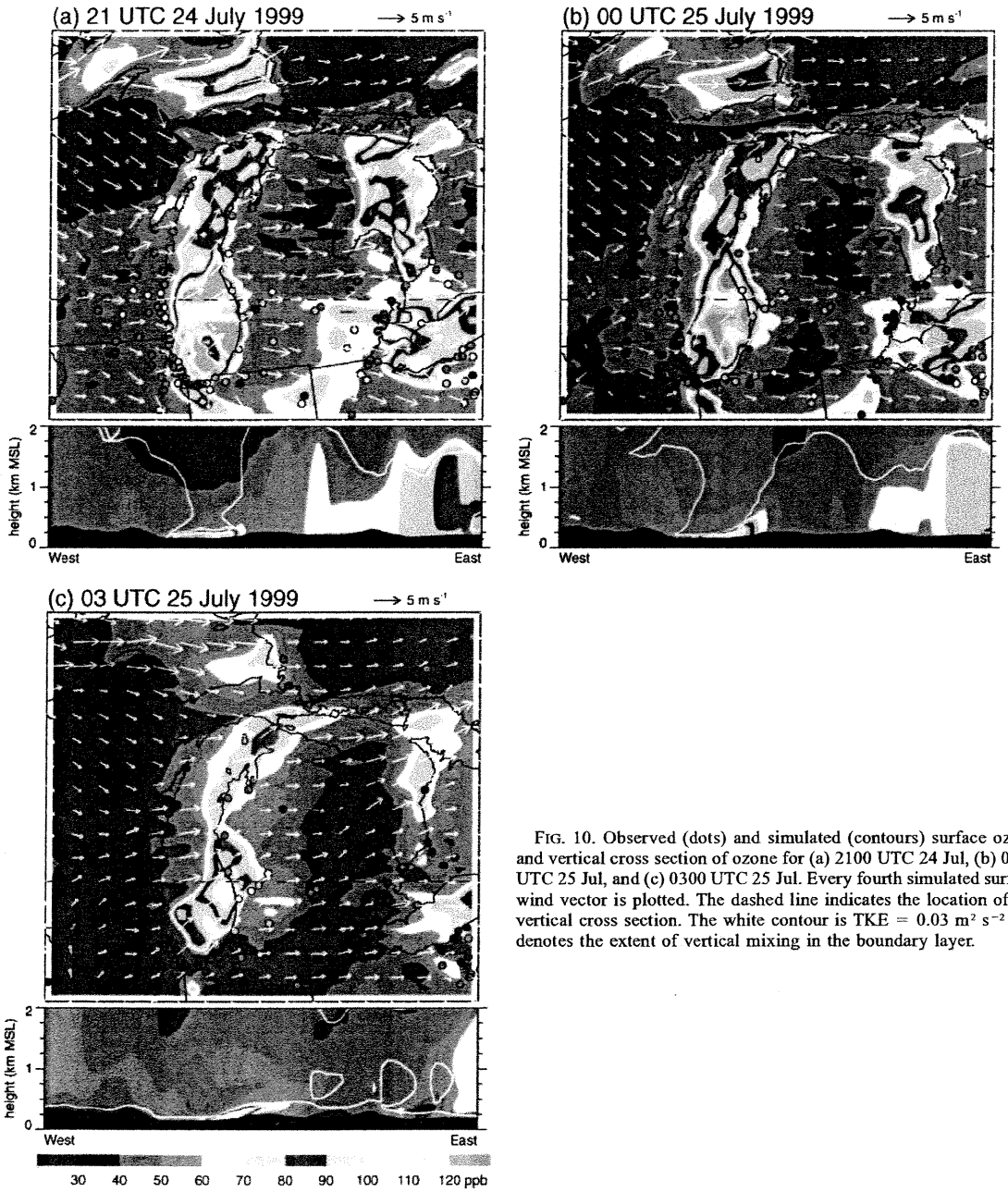

FIG. 10. Observed (dots) and simulated (contours) surface ozone and vertical cross section of ozone for (a) 2100 UTC 24 Jul, (b) 0000 UTC 25 Jul, and (c) 0300 UTC 25 Jul. Every fourth simulated surface wind vector is plotted. The dashed line indicates the location of the vertical cross section. The white contour is TKE = 0.03 $m^2 s^{-2}$ and denotes the extent of vertical mixing in the boundary layer.

on 24 July was consistent with the ferry data, as shown in Fig. 11, except during the late afternoon. While the observed and predicted ozone was between 70 and 90 ppb over the middle of the lake during the midafternoon between 1900 and 2000 UTC, the predicted values on the eastern side of the lake were higher than observed between 2100 and 2200 UTC.

Vertical profiles of temperature, potential temperature, turbulence kinetic energy (TKE), ozone, NO_x, NO_z, and tendency terms on 24 July are shown in Fig. 12 to illustrate the cause for the high ozone mixing ratios over the lakes. Here, NO_z is defined as sum of all NO_x oxidation products, including nitric acid (HNO_3), nitrous acid (HONO), nitrate radical (NO_3), dinitrogen pentoxide (N_2O_5), and peroxyacetyl nitrate (PAN). The profiles are taken from a grid point in the center of Lake Michigan along the vertical cross section shown in Fig. 10a. Between 1200 and 2100 UTC an inversion was

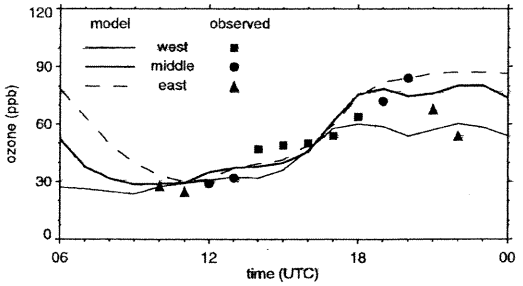

FIG. 11. Observed and simulated ozone over Lake Michigan on 24 Jul averaged over the western, middle, and eastern regions denoted in Fig. 9.

present with temperatures 2°–3°C higher 150 m above the lake (Fig. 12a). The potential temperature profiles also show the stable layer adjacent to the lake. Although the temperatures increase during the day, they do so nearly uniformly aloft so that the stability remains nearly the same during the day. Small values of TKE were produced near the surface (Fig. 12b), indicating that pollutants would be trapped within the shallow surface layer. In the morning at 1200 UTC, ozone was reduced to 20 ppb near the surface by NO titration (Fig. 12c). A NO_x/NO_z ratio of 2.3 was produced in the morning, indicating the presence of fresh emissions. By the afternoon at 2100 UTC, ozone mixing ratios within the shallow layer increased dramatically to 135 ppb. During the day, NO_x diminished and NO_z increased, indicative of the photochemical activity that produced the ozone (Figs. 12d and 12e). At 2100 UTC, the NO_x/NO_z ratio decreased to 0.15. The tendency terms of the governing ozone equation accumulated between 1200 and 2100 UTC (Fig. 12f) show that chemical production was the dominant term near the surface (198 ppb). This high chemical production of ozone was offset by losses through horizontal advection (−40 ppb), vertical transport (−25 ppb), and deposition (−42 ppb).

As the CBL began to collapse by 0000 UTC (Fig. 10b), vertical mixing was reduced and relatively higher surface ozone mixing ratios were produced further inland over southeast Michigan. The modeling system indicates that the high ozone mixing ratios observed over western Michigan on this day resulted from a combination of local emissions and emissions transported

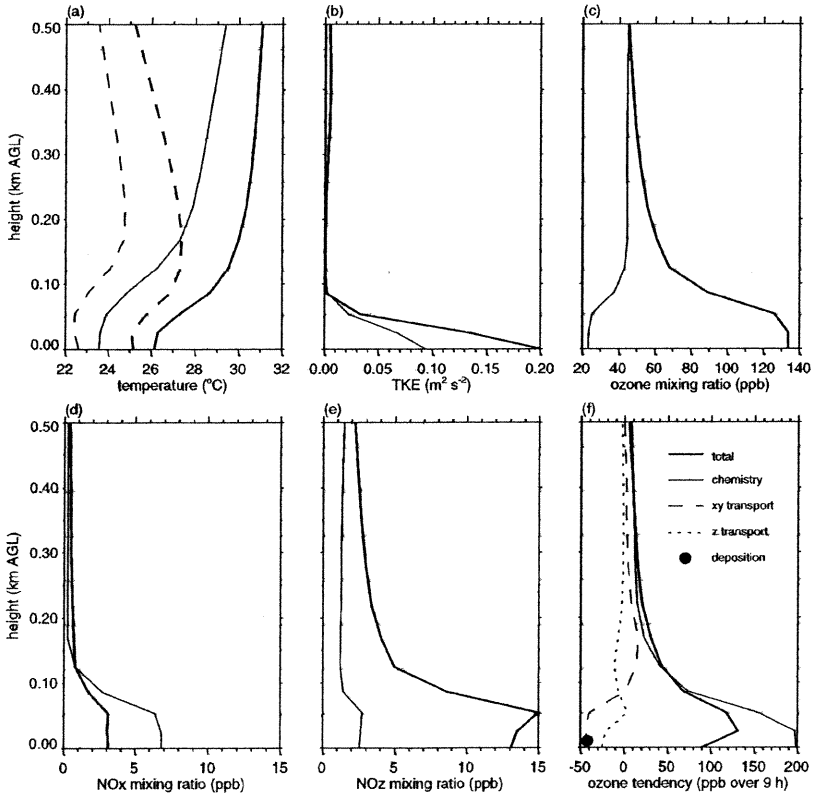

FIG. 12. Vertical profile of simulated (a) temperature (dashed) and potential temperature (solid), (b) TKE, (c) ozone, (d) NO_x, and (e) NO_z over the middle of Lake Michigan along the vertical cross section in Fig. 10 at 1200 UTC (thin line) and 2100 UTC (thick line) 24 Jul. (f) The ozone tendency due to chemistry, horizontal (xy) transport, vertical (z) transport, and deposition over the 9-h period between 1200 and 2100 UTC 24 Jul is shown.

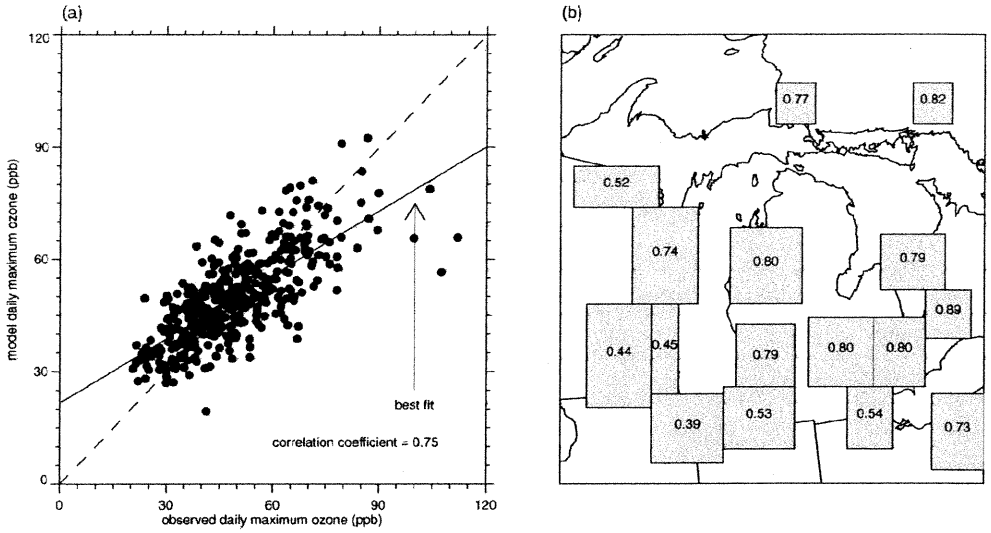

FIG. 13. (a) Observed vs simulated daily maximum ozone mixing ratios for all 16 regions and (b) correlation coefficient of the observed and simulated daily ozone maximum for each region between 17 Jul and 14 Aug 1999.

from Milwaukee and Chicago. A stable boundary layer (SBL) formed by 0300 UTC (Fig. 10c) so that ozone near the surface was reduced by NO titration, while the higher concentrations of ozone over the lake during the afternoon were advected over the SBL. The lowest surface ozone mixing ratios occurred over the urban areas where the NO emissions were the highest. Figure 10 shows that at specific locations, relatively larger errors were produced by the model. For example, ozone around Detroit was much higher than observed at 0000 UTC but was close to the observed values at 0300 UTC. This suggests that the predicted collapse of the CBL occurred an hour or two later than observed in this area.

Production of ozone over the lake and near-surface transport over the eastern shore, such as the case on 24 July (Fig. 10), was simulated on a number of days during the 30-day period. On other days, ozone produced over Milwaukee and Chicago was mixed upward within the CBL and a convergence zone produced by a lake-breeze circulation. During the evening the ozone aloft was transported by westerly winds and entrained in the growing CBL the subsequent day over downwind locations such as Michigan and Ontario, Canada.

c. *Air chemistry statistics*

In this section the performance of the model in simulating ozone is quantified. A scatterplot of the observed and simulated daily maximum ozone mixing ratios from the four regions in Fig. 8 and the other 12 regions is shown in Fig. 13a. The simulated maximum was too low in a few instances where the observed ozone exceeded 90 ppb in regions 8 and 9, and the simulated maximum was a few parts per billion too high when the observed maximum was below 40 ppb. A correlation coefficient between the observed and simulated maximum daily ozone over the whole domain was 0.75 with values in individual ranging from 0.89 to 0.39 (Fig. 13b). This indicates that in many regions the model captured the majority of the observed multiday variance over the 30-day period. Over the ferry transects (Fig. 9) a correlation coefficient of 0.66 was obtained, but there were fewer observations to evaluate the simulated temporal variability ozone over the lake.

Figure 14 depicts the bias, $\overline{\text{simulated} - \text{observed}}$, and gross error, $\overline{|\text{simulated} - \text{observed}|}$, over the simulation period for the 1-h daily maximum, 8-h average daily maximum (Chamedies et al. 1997), and the 1-h daily minimum for each of the 16 regions. The results are also listed in Table 2. The bias in the simulated 1-h peak ozone mixing ratio was very low, between -1 and 5 ppb, in most of the northern two-thirds of the domain, except in region 6 around Sault Ste. Marie, which had a bias of 6.9 ppb. In the southern third of the domain, the model usually underpredicted the 1-h peak values, with a bias as much as -5.3 ppb in region 9 and a gross error of 10.7 ppb in region 5. The bias in the 8-h maximum shows a similar pattern to the 1-h bias. The statistics showed that the largest underprediction in the maximum ozone mixing ratio usually occurred downwind of Chicago, the area with the highest precursor emission rates. In contrast, the urban areas in the southern third of the domain had a very low bias in the 1-h minimum values between -3 and 3 ppb, while the downwind rural areas consistently overpredicted the minimum value. The largest 1-h minimum bias was as high as 17 ppb in regions 6 and 7. One-half of the values for the 1- and 8-h maximum bias and five of the values for the 1-h minimum bias were not statistically signif-

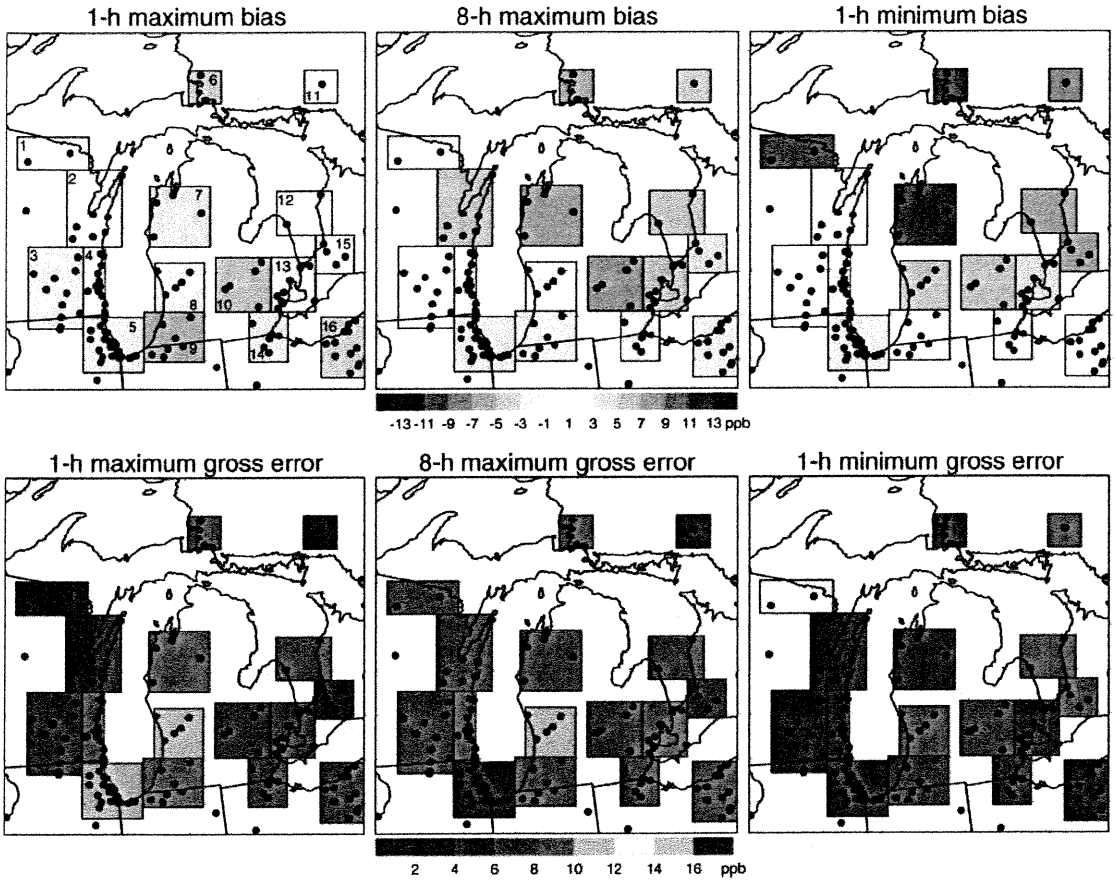

FIG. 14. Average bias and gross error of the 1- and 8-h maximum and 1-h minimum ozone mixing ratios between 17 Jul and 14 Aug 1999 for the 16 geographic regions.

TABLE 2. Bias and gross error in predicted ozone over the simulation period between 17 Jul and 14 Aug 1999.

Region	1-h max bias	8-h max bias	1-h min bias	1-h max gross error	8-h max gross error	1-h min gross error
1	−0.57*	2.58*	12.00	5.77	6.34	12.77
2	2.93	5.37	2.91	5.86	7.28	5.78
3	−2.40*	−0.04*	−0.30*	7.42	6.65	5.84
4	2.04*	2.93*	1.37*	8.61	9.44	5.92
5	−1.61*	−1.10*	−2.37	10.70	10.31	4.27
6	6.89	8.96	16.25	7.75	9.23	16.25
7	4.34	7.07	16.94	8.01	9.45	16.99
8	−1.43	1.86*	5.31	10.37	10.34	7.04
9	−5.30	−2.15*	0.54*	9.99	8.43	4.90
10	5.11	8.85	6.69	6.87	9.26	7.80
11	2.43	5.22	9.66	4.18	5.97	9.75
12	2.24*	5.61	8.01	8.69	7.95	9.05
13	2.80*	6.88	3.61	7.85	9.00	5.66
14	−1.16*	2.71*	1.81*	6.86	6.56	4.46
15	1.31*	4.17	7.99	5.72	5.99	9.72
16	−4.69	−1.62*	−0.73*	7.26	6.33	5.24

* Not statistically significant using a Student's t test with $\alpha = 0.05$.

icant using the Student's t test with $\alpha = 0.05$. All of the gross errors, however, were statistically significant.

While the predicted ozone distribution was similar to observations in most locations, the ozone mixing ratios were underpredicted at stations located over southwestern Michigan and northern Indiana not adjacent to Lake Michigan. This type of error occurred on a number of days, resulting in the negative bias in the 1-h daily maximum shown in Fig. 14. Uncertainties associated with the local emissions in this area may be one reason for the low simulated ozone production. The NO_x emissions may be too high and/or volatile organic compound (VOC) emissions may be too low. Unfortunately, the specific reason for the underprediction in ozone cannot be determined because of a lack of meteorological and chemical measurements aloft in this area.

In contrast with the previous evaluations that divided the results into 16 regions, the bias and gross error shown in Fig. 15 are based on up to 109 EPA and 10 Canadian monitoring stations and the grid point closest to those stations. The 8-h average daily maximum employed concentrations 4 h before and after the time of the daytime peak value. The observed average 1- and 8-h maximum ozone mixing ratios are also shown because the magnitudes of the bias and gross error are usually higher during the regional high ozone episodes. When multiple ozone monitoring stations occurred within a grid cell (usually in urban areas), the average value was employed for the statistical analysis. Because some "spinup" time is required to obtain realistic model results, the statistics for the first two afternoons are not plotted. The average daily maximum values over the domain were usually well predicted. Prior to 28 July, the 1- and 8-h bias was usually between −5 and 5 ppb. When regional-scale high ozone episodes occurred on 29 and 30 July, the simulated ozone was 15 ppb lower than that observed on average. After a cold front moved though the area on 31 July, the average ozone mixing ratios decreased and the absolute value of the bias dropped to 10 ppb or less. The daily values of the bias and gross error for the 1- and 8-h peak ozone mixing ratios are similar to those obtained by other chemical models, but the minimum values are considerably lower than the 10–20 ppb reported in the literature (NARSTO 2001). Here, the minimum ozone values were between 0 and 5 ppb too high on average, with the exception of 30 and 31 July.

d. Ozone exposure

Because the model reproduced many features of the ozone time series (Fig. 8) and the observed ozone distribution (Figs. 9 and 10), we computed the ozone exposure to determine the overall effect of ozone production resulting from sources in the Great Lakes region. The number of hours during the simulation period that exceeded 60 and 80 ppb is shown in Fig. 16. These two criteria have been frequently used in the literature to determine the impact of ozone on forest vegetation. The simulated distribution is consistent with the observations in most locations. The highest exposures occurred over the lakes because of the simulated high ozone production rates within the stable boundary layer on many days. Some of the highest observed ozone exposures occurred along the lake shore as well. The observed and simulated 60-ppb exposures were between 110 and 130 h along southern Lake Huron and between 90 and 110 h along southeastern Lake Michigan (Fig. 16a). However, some differences between the observed and simulated exposures along the lake shores is expected because the 12-km horizontal grid spacing will not represent sharp gradients in meteorological and chemical fields that can occur in these areas. For example, the 60-ppb ozone exposures over northwestern Indiana were too low, but there were higher simulated values a few kilometers north over the lake. Over the northeastern shore of Lake Michigan, predicted 60-ppb ozone exposure was higher than observed, indicating that the model usually advected ozone too far inland in that location. The underestimation of ozone exposure at the four stations located in northern Indiana within region 9 was due to the low simulated peak ozone mixing ratios, similar to the results shown in Fig. 10.

As shown in Fig. 16b, only a few stations have a significant number of hours greater than 80 ppb. The model results also reproduce this feature, with the highest ozone exposures over land along the lake shores. The simulated ozone exposures were greater than 80 ppb between 25–45 h over southeastern Lake Michigan, similar to the observations along the lake shore. The downwind urban plume from Detroit was reproduced with an ozone exposure between 35 and 45 h. The observed ozone exposure at two stations in southern Lake Huron was between 35 and 45 h, but the simulated results were too low. The 80-ppb ozone exposures in the region will be significantly higher, however, when the overall meteorological conditions are more favorable to ozone production.

Interestingly, the highest simulated ozone exposures over land occur in areas where no monitoring stations are located. Ozone monitoring stations are usually located near cities with relatively high emission rates of NO_x. Near these stations NO titration would tend to reduce ozone mixing ratios, and higher ozone mixing ratios would occur downwind in more rural locations.

4. Sensitivity simulations

a. Effect of lake temperature

Lake temperatures in mesoscale and air quality model applications are usually based on monthly climatological values in which the magnitude and distribution can differ substantially from the observed daily values. Because the model predicted relatively high values of ozone over each of the lakes, an additional sensitivity

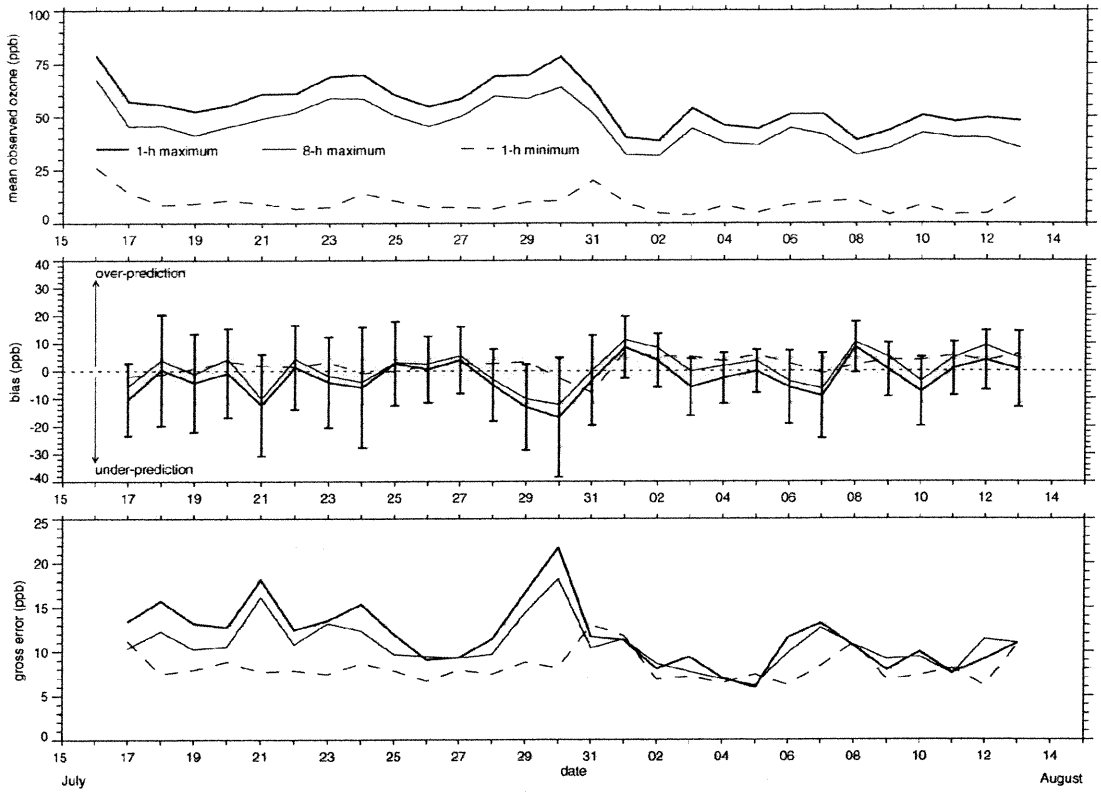

FIG. 15. Mean observed ozone, bias, and gross error of the 1- and 8-h maximum and 1-h minimum ozone mixing ratios averaged over grid 3. Vertical lines in the middle plot are 1 standard deviation of the 1-h maximum.

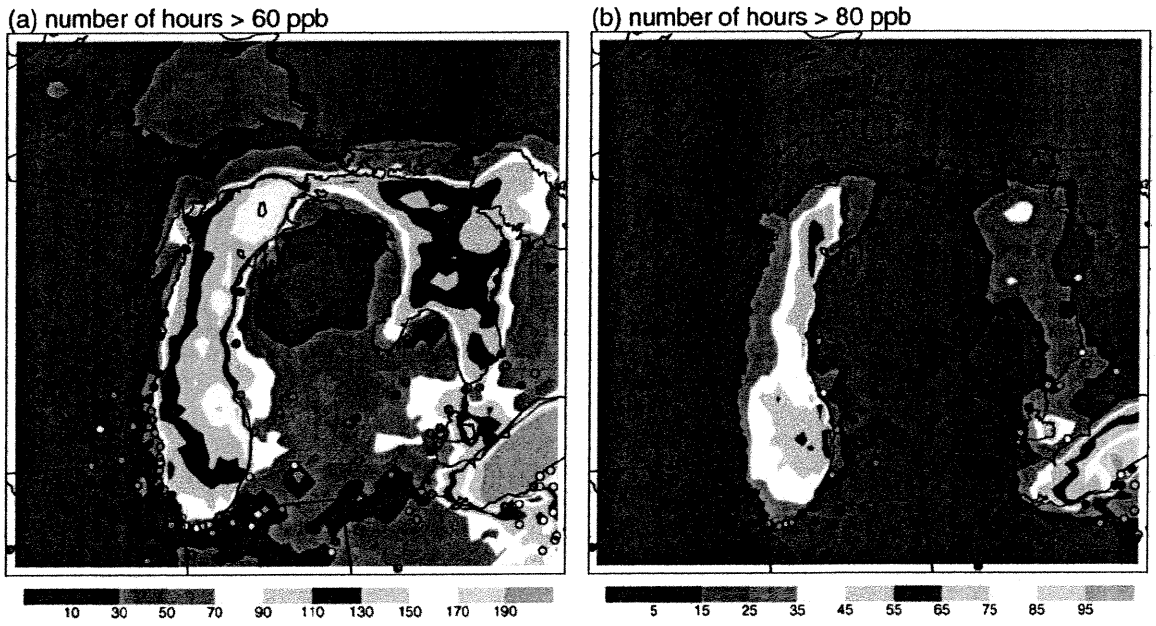

FIG. 16. Spatial distribution of observed (dots) and predicted (contours) ozone exposure based on the number of hours during the 30-day period greater than (a) 60 and (b) 80 ppb.

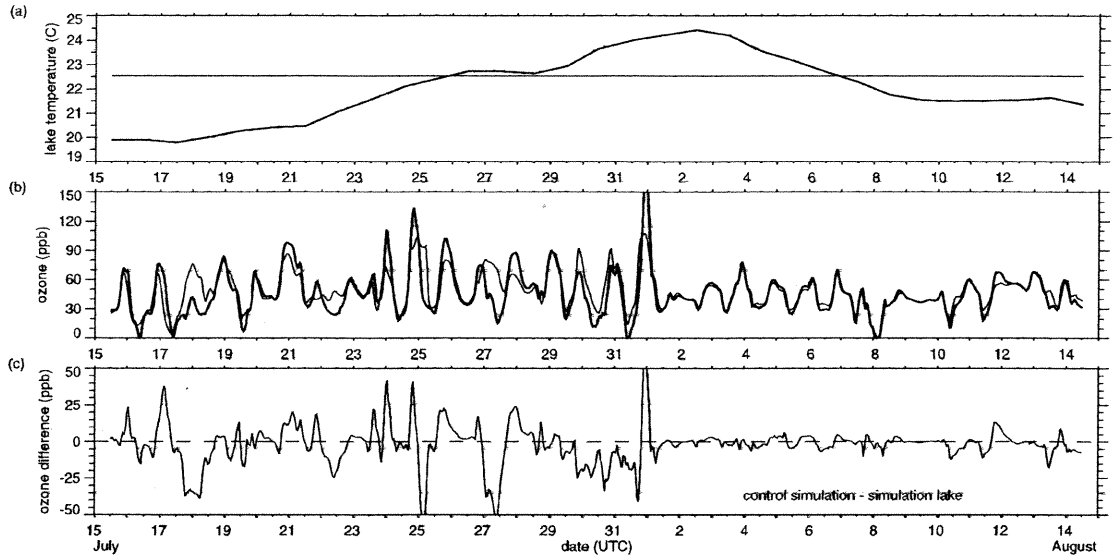

FIG. 17. Time series of (a) surface lake temperature and (b) ozone in the middle of Lake Michigan along the vertical cross section in Fig. 10 from the control simulation (thick line) and simulation lake (thin line). (c) Difference in ozone between the two simulations.

simulation, *simulation lake,* was carried out to examine the effect of lake temperature on ozone production. The mesoscale model run was repeated, except that the average climatological lake temperatures for July and August were employed and held constant during the simulation period. The climatological distribution had a gradual south–north variation but lacked most of the small-scale west–east variations shown in Fig. 2b. While the climatological lake temperatures were within a few degrees of the observed temperatures over Lake Superior, the lake temperatures over southern Lake Michigan and Lake Erie were as much as 15°C too low. These cooler temperatures that persisted over the 30-day period would have a profound effect on the simulated meteorological conditions around the lakes. Instead, we wanted to examine the effect of smaller departures in temperature on meteorological conditions and ozone production. Therefore, the climatological temperature distribution in simulation lake was raised by 8°C. The spatial temperature distribution then became more similar to the mean temperatures derived from satellite measurements over the 30-day period.

An example of the lake temperatures employed from the *control simulation* and simulation lake in the middle of southern Lake Michigan is shown in Fig. 17a. At this location, the temperature employed by simulation lake was 22.5°C. Between 15 and 21 July, the observed lake temperatures were about 2.5°C lower than the temperatures from simulation lake. The observed lake temperatures gradually rose during the period so that they were as much as 2°C warmer than simulation lake between 1 and 4 August. After 4 August, the observed temperatures slowly decreased so that they became about 1°C lower than those from simulation lake.

As expected, changing the lake temperature had an effect on the simulated shallow stable layers over water. Prior to 1 August, there were a number of days in which the near-surface stability was significantly different between the two simulations. For example, the temperature inversion base during the afternoon of 24 July simulation lake was about 100 m higher than from the control simulation shown in Fig. 12a. After 1 August, the differences in stability from both simulations were small because of a greater influence of synoptic forcing on the evolution of the boundary layer. Occasionally the winds and temperatures over adjacent land areas in simulation lake were noticeably different than the control simulation, but the impacts were transient. The overall statistics and comparisons with meteorological observations over land (such as Figs. 4, 5, and 6) were similar to the control simulation.

The change in near-surface temperature, however, had a dramatic impact on ozone production over the lakes. A comparison of the predicted ozone in the middle of Lake Michigan from the two simulations is shown in Figs. 17b and 17c. On 6 days prior to 1 August, ozone from the control simulation is 10–40 ppb higher than from simulation lake, while ozone from simulation lake was higher than the control simulation on 4 days. Changes in local stability may be one factor contributing to the differences in ozone. For example, the deeper mixing depth on 24 July in simulation lake was consistent with the lower ozone mixing ratios at this time. Other factors, such as changes in cloudiness and their effect on photolysis rates, may contribute to the differences in the simulations. After 1 August, the series of synoptic systems that passed over the region produced meteorological conditions that were less favorable for

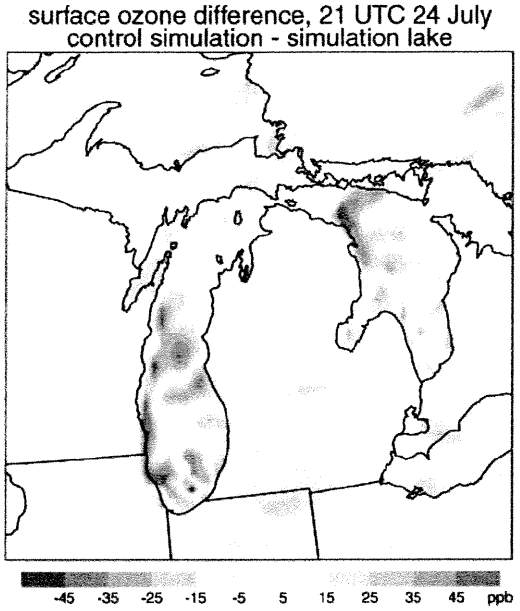

FIG. 18. Difference in surface ozone between the control simulation and simulation lake at 2100 UTC 24 Jul 1999.

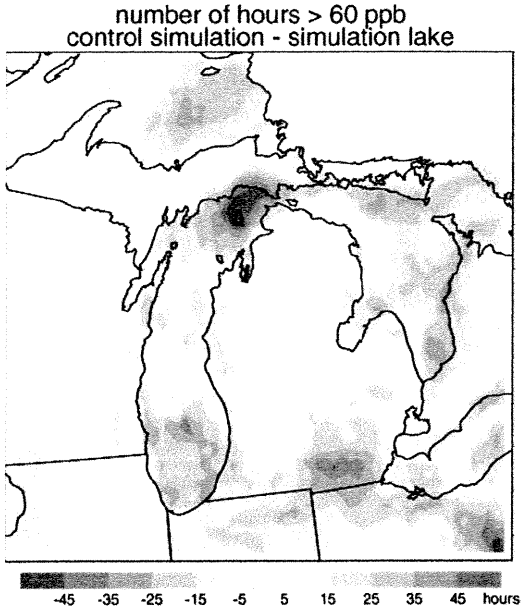

FIG. 19. Differences in the spatial distribution of predicted ozone exposure based on the number of hours during the 30-day period greater than 60 ppb (control simulation − simulation lake).

ozone production in the region. While there were still stable conditions simulated over the lake, the stability was lower so that there was additional loss due to vertical transport in comparison with Fig. 12f. The series of cold fronts also advected ozone produced over the lake out of the western Great Lakes region on a daily basis so that no multiday accumulation of pollutants occurred.

There also appeared to be no correlation of the differences in lake temperature and ozone, as shown in Fig. 17. This is probably due to the spatial inhomogeneity in the observed lake temperatures. For example, while lake temperature in this location from the control simulation and simulation lake were similar between 24 and 28 July, the lake temperatures were significantly different at other locations. These spatial differences affect the overall ozone production over the lake. An example of the differences in surface ozone at 2100 UTC 24 July between the two simulations is shown in Fig. 18. Ozone from the control simulation was as much as 45 ppb higher in three areas of southern Lake Michigan and 45 ppb lower along the western shore of Lake Michigan. The NO titration reduced ozone along the western shore because relatively low lake temperatures (Fig. 2b) increased the local stability near the high emission sources. Surprisingly, lake temperatures affected ozone mixing ratios over the land areas by 5–15 ppb. These differences were not due to direct changes in the local meteorological conditions, but to changes in ozone over the lake that was subsequently advected over land.

The difference in the spatial distribution of ozone exposure (control simulation − simulation lake) based on the number of hours greater than 60 ppb is shown in Fig. 19 to illustrate the overall effect of lake temperatures during the 30-day period. When compared with the control simulation (Fig. 16a), constant lake temperatures result in somewhat higher number of hours greater than 60 ppb over southeastern Lake Michigan and much lower values over northern Lake Michigan, Lake Huron, and Lake Superior. This pattern corresponds to the differences in lake temperatures between the two simulations, where the temperatures from simulation lake were warmer over the northern areas and colder over the southern areas than the control simulation. The colder lake temperatures over southern Lake Michigan produced stronger stable boundary layers, less vertical mixing, and, consequently, more ozone. Somewhat longer periods of higher ozone mixing ratios also occurred over southern Michigan, Indiana, and Ohio, indicating the indirect effect of the lake temperatures on the land areas.

b. Effect of emission rates

Population and land use changes will affect the rates of anthropogenic and biogenic emissions and, subsequently, the amount of ozone produced. To determine the effect of changing emission patterns for the given meteorological conditions between 15 July and 14 August 1999, four sensitivity simulations were performed with the chemical transport model using the same meteorology. Simulation N50V100I100 reduced NO_x emissions at all grid points and at all times of the day by 50%, while the other species remain the same. Likewise, sim-

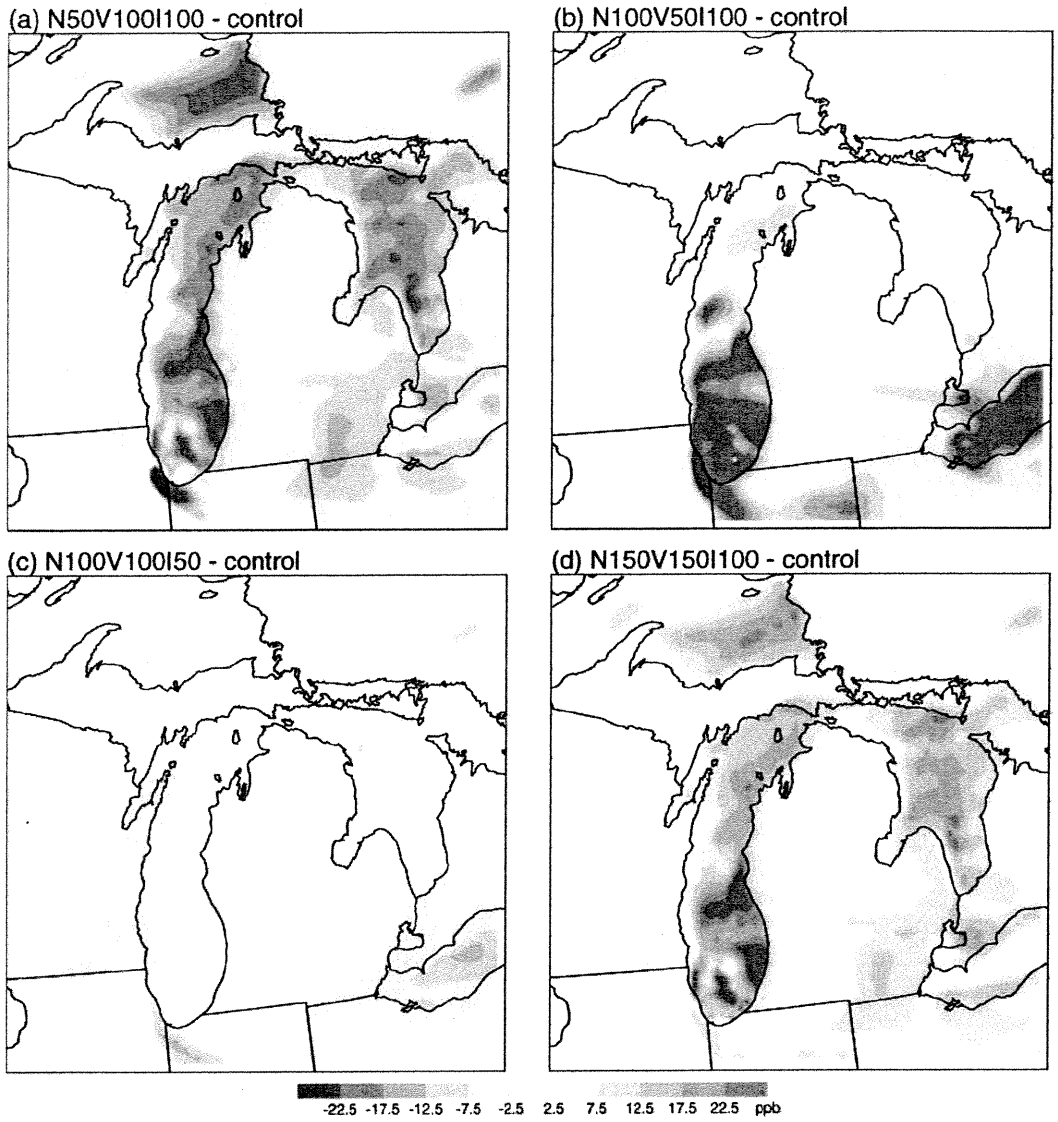

FIG. 20. Difference in the simulated surface ozone at 2100 UTC 24 Jul between the control simulation and emission sensitivity simulations (a) N50V100I100, (b) N100V50I100, (c) N100V100I50, and (d) N150V150I100.

ulation N100V50I100 reduced VOC emissions by 50% while other emissions remained the same. These two simulations were performed to examine the effect of emission-control strategies that might be employed. Simulation N100V100I50 reduced the isoprene emissions by 50% to examine the effect of reduced forest cover. The fourth simulation, simulation N150V150I100, increased both NO_x and VOCs by 150% to represent growth with no emission-control strategies.

Differences in surface ozone concentrations between the four sensitivity simulations and the control simulation at 2100 UTC 24 July are shown in Fig. 20. The sensitivity simulations affect the ozone mixing ratios in a manner similar to other NO_x and VOC simulations (Sillman 1999). For a reduction of NO_x (Fig. 20a), ozone was reduced downwind of the major urban centers, while ozone increased directly over Chicago. Peak values of ozone over Lake Superior, Lake Huron, and northern Lake Michigan were reduced from 95 ppb to around 75 ppb. Over southern Lake Michigan and Lake Erie, ozone was reduced by 5–10 ppb. When VOCs were reduced in simulation N100V50I100 (Fig. 20b), ozone in southern Lake Michigan and Lake Erie was reduced significantly, while ozone over more remote regions was reduced only slightly. Ozone over the land areas was similar to that in the control simulation. Reducing isoprene emission rates in simulation N100V100I50 (Fig. 20c) only reduced ozone in most locations by a few

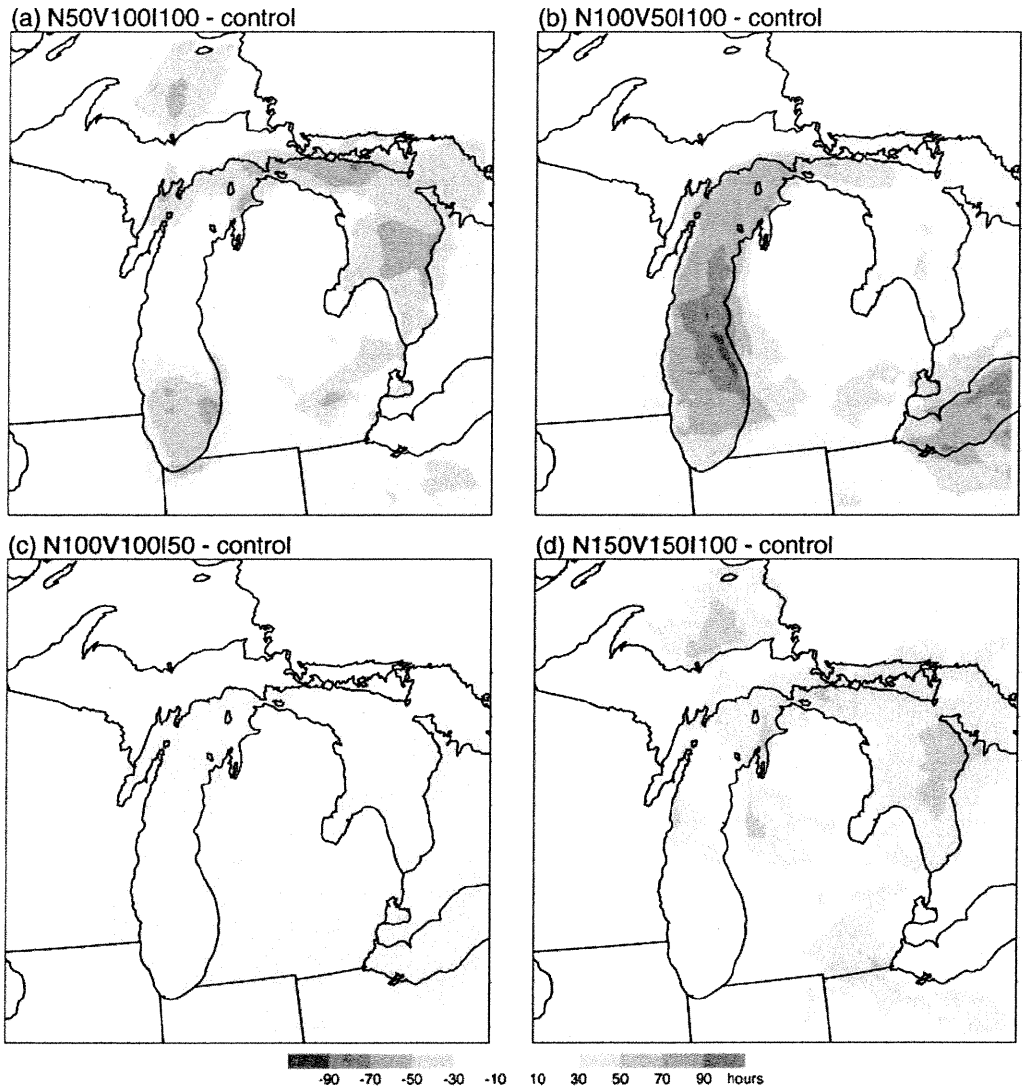

FIG. 21. Differences in 60-ppb ozone exposure between the control simulation and emission sensitivity simulations (a) N50V100I100, (b) N100V50I100, (c) N100V100I50, and (d) N150V150I100.

parts per billion. The exception was over Lake Erie, where ozone mixing ratios were reduced by as much as 10 ppb. In the simulation with projected growth in the emissions, simulation N150V150I100 (Fig. 20d), ozone increased nearly everywhere. The region over Lake Michigan with mixing ratios greater than 120 ppb in the control simulation increased dramatically. While ozone mixing ratios along the eastern shore increased as well, convective boundary layer processes still mixed ozone advected over land so that the modest increases in ozone over Michigan were due to local emissions.

The effect of modified emission rates shown in Fig. 20 were consistent throughout the simulation period, as shown by the differences in the 60-ppb ozone exposure between the sensitivity simulations and the control simulation in Fig. 21. The reduction in NO_x increased the number of hours greater than 60 ppb over southern Lake Michigan by as much as 80 h, while the number of hours in remote locations was reduced by 10–60 (Fig. 21a). Reducing VOC emission rates reduced ozone exposure everywhere, with the greatest reductions in east-central Lake Michigan and over Lake Erie that are located just downwind of major urban areas (Fig. 21b). A reduction of isoprene emission rates decreased ozone exposure by only 10–30 h (Fig. 21c). Interestingly, the ozone exposure changes were relatively minor where the isoprene emission rates were the highest (Fig. 3b), because the meteorological conditions in the northern forested areas were not favorable for high ozone concentrations, even in the control simulation. An increase

in NO_x and VOCs (Fig. 21d) lead to 10–70 more hours of ozone exceeding 60 ppb. The highest increases were in downwind regions, while only small increases occurred directly over the major urban areas.

5. Summary

A coupled meteorological and chemical modeling system was used to simulate the evolution of ozone over the western Great Lakes region between 15 July and 14 August 1999. A reasonable agreement between the control simulation and observations was obtained in most locations, and sensitivity simulations have been employed to examine the effect of lake temperature and emissions on the distribution of ozone in the region. The principal findings from this study are the following:

1) The average bias for ozone over the domain during the 30-day period was −1.3 ppb for the peak 1-h value during the day and 5.5 ppb for the minimum value at night. The largest errors in the daily 1-h maximum ozone occurred over northern Indiana and southeastern Michigan, downwind of pollutants emitted from the Chicago area, while the largest errors in the daily 1-h minimum ozone occurred in remote downwind locations in northern Michigan and Wisconsin.
2) High ozone mixing ratios were frequently produced over the lake surfaces, even when meteorological conditions over land were not conducive to ozone production. Ozone mixing ratios within a shallow layer of the lake surface often exceeded the National Ambient Air Quality Standard of 125 ppb. Southwesterly winds advected the polluted air over western Michigan, but mixing within the deep CBL several kilometers inland then significantly diluted the concentration of ozone. After the collapse of the CBL, surface ozone concentrations remained relatively high.
3) Simulated ozone exposure compared well with the observed data in most locations.
4) Ozone production over the lakes was very sensitive to lake temperature. Changing the lake temperatures by 5°C changed ozone mixing ratios by as much as 50 ppb. The effect of lake temperatures had a smaller effect when stronger synoptic forcing was present after 1 August. The lake temperatures also had an indirect effect on ozone mixing ratios over land, which was usually less than 10 ppb. The difference in 60-ppb ozone exposure along the shore of northern Lake Michigan between the two lake temperature scenario simulations was as high as 60 h over the 30-day period.
5) Reducing NO_x emission rates lead to higher ozone in southern Lake Michigan, immediately downwind of Chicago and Milwaukee, and lower ozone in more remote areas. Reducing VOC emissions rates lead to lower ozone mixing ratios everywhere. The results were not very sensitive to isoprene emissions. Increases in both NO_x and VOCs lead to higher ozone concentrations at downwind locations. The sensitivity simulation showed that ozone exposures in remote forest regions will increase if growth patterns continue.

Air quality and landscape change are usually treated as separate issues; however, they are closely coupled through dynamical, radiative, and chemical processes. Research on the complex linkages between landscape change and regional air quality has just begun. Global- and regional-scale climate predictions indicate that human activities will significantly change the average meteorological conditions over the next several decades. Changes in meteorological parameters, such as temperature, humidity, clouds, and precipitation, will also affect the emissions, chemical transformation, transport, vertical mixing, and deposition of air pollutants. Future regional-scale predictions of ozone will also depend upon the assumptions of population, economic development, land use patterns, and technology employed by primary pollutant emissions projections that are highly uncertain. The magnitude and spatial distribution of anthropogenic and biogenic primary emission rates will likely change with time as the result of urban sprawl and the rapid growth of rural areas. For example, the modeling study of Civerolo et al. (2000) demonstrated that surface ozone concentrations during one air pollution episode in the northeastern U.S. urban corridor were sensitive to land use changes.

While a range of meteorological conditions were simulated during the 30-day period in this study, the effect of changing emissions on future ozone exposure is more complex in the context of climate and landscape change. The large bodies of water in the region are a factor that needs to be considered when making future ozone exposure estimates. Global- and regional-scale climate models do not represent the lakes or poorly resolve the lakes. Average increases in air temperature due to climate change will also affect the seasonal variation of land and lake temperatures. This will subsequently affect the development of the stable boundary layer and ozone production rates over the lake surfaces. Our study shows that changing the lake temperatures by a few degrees can have a profound effect on the ozone concentrations. Thus, a more complete understanding of future air quality in the region will require a coupled meteorological–lake modeling system.

Acknowledgments. We thank David Schwab of NOAA GRERL for his assistance in obtaining Great Lakes temperature data, Bill Adamski and Timothy Trapp of the Wisconsin Department of Natural Resources for providing the *Badger* ferry ozone data, and Chris Doran of Pacific Northwest National Laboratory for his comments on this manuscript. This research was supported by the USDA Forest Service under an inter-

agency agreement NC-96-01-IA and by the U.S. Department of Energy under the auspices of the Atmospheric Sciences Program of the Office of Biological and Environmental Research. Pacific Northwest National Laboratory is operated for the DOE by Battelle Memorial Institute under contract DE-AC06-766RLO 1830.

REFERENCES

Armentano, T. V., and E. S. Menges, 1987: Air-pollution-induced foliar injury to natural populations of jack and white pine in a chronically polluted environment. *Water Air Soil Pollut.*, **33,** 395–409.

Bennett, J. P., P. Rassat, P. Berrang, and D. F. Karnosky, 1992: Relationships between leaf anatomy and ozone sensitivity of *Fraxinus pennsylvanica Marsh.* and *Prunus serotina Ehrh. Environ. Exp. Bot.*, **32,** 33–41.

——, R. L. Anderson, M. L. Mielke, and J. J. Ebersole, 1994: Foliar injury air pollution surveys of eastern white pine (*Pinus strobus L.*): A review. *Environ. Monit. Assess.*, **30,** 247–274.

Carroll, M., S. B. Bertman, and P. B. Shepson, 2001: Overview of the Program for Research on Oxidants: Photochemistry, Emissions, and Transport (PROPHET) summer 1998 measurements intensive. *J. Geophys. Res.*, **106,** 24 275–24 288.

Chamedies, W. L., R. D. Saylor, and E. B. Cowling, 1997: Ozone pollution in the rural U.S. and new NAAQS. *Science,* **276,** 916.

Chang, J. S., R. A. Brost, I. S. A. Isaksen, S. Madronich, P. Middleton, W. R. Stockwell, and C. J. Walcek, 1987: A three dimensional Eulerian acid deposition model: Physical concepts and formulation. *J. Geophys. Res.*, **92,** 14 681–14 700.

Civerolo, K. L., G. Sistla, S. T. Rao, and D. J. Nowak, 2000: The effects of land use in meteorological modeling: Implications for assessment of future air quality scenarios. *Atmos. Environ.*, **34,** 1615–1621.

Coleman, M. D., J. G. Isebrands, R. E. Dickson, and D. F. Karnosky, 1995: Photosynthetic productivity of aspen clones varying in sensitivity to tropospheric ozone. *Tree Physiol.*, **15,** 585–592.

Cooper, O. R., J. L. Moody, T. D. Thornberry, M. S. Town, and M. A. Carroll, 2001: PROPHET 1998 meteorological overview and air-mass classification. *J. Geophys. Res.*, **106,** 24 289–24 299.

Dye, T. S., P. T. Roberts, and M. E. Korc, 1995: Observations of transport processes for ozone and ozone precursors during the 1991 Lake Michigan Ozone Study. *J. Appl. Meteor.*, **34,** 1877–1889.

Eastman, J. L., R. A. Pielke, and W. A. Lyons, 1995: Comparison of lake-breeze model simulations with tracer data. *J. Appl. Meteor.*, **34,** 1398–1418.

Fast, J. D., 1995: Mesoscale modeling in areas of highly complex terrain employing a four-dimensional data assimilation technique. *J. Appl. Meteor.*, **34,** 2762–2782.

——, R. A. Zaveri, X. Bian, E. G. Chapman, and R. C. Easter, 2002: The effect of regional-scale transport on oxidants in the vicinity of Philadelphia during the 1999 NE-OPS field campaign. *J. Geophys. Res.*, **107,** 4307, doi:10.1029/2001JD000980.

Gery, M. W., G. Z. Whitten, J. P. Killus, and M. C. Dodge, 1989: A photochemical kinetics mechanism for urban and regional scale computer modeling. *J. Geophys. Res.*, **94,** 12 925–12 956.

Hanna, S. R., and J. C. Chang, 1995: Relations between meteorology and ozone in the Lake Michigan region. *J. Appl. Meteor.*, **34,** 670–678.

——, and R. Yang, 2001: Evaluations of mesoscale models' simulations of near-surface winds, temperature gradients, and mixing depths. *J. Appl. Meteor.*, **40,** 1095–1104.

——, G. E. Moore, and M. E. Fernau, 1996: Evaluation of photochemical grid models (UAM-IV, UAM-V, and the ROM/UAM-IV couple) using data from the Lake Michigan Ozone Study (LMOS). *Atmos. Environ.*, **30,** 3265–3279.

Helfand, H. M., and J. C. Labraga, 1988: Design of a nonsingular level 2.5 second-order closure model for the prediction of atmospheric turbulence. *J. Atmos. Sci.*, **45,** 113–132.

Houyoux, M. R., J. M. Vukovich, C. J. Coats Jr., N. W. Wheeler, and P. S. Kasibhatla, 2000: Emission inventory development and processing for the Seasonal Model for Regional Air Quality (SMRAQ) project. *J. Geophys. Res.*, **105,** 9079–9090.

Karnosky, D. F., R. E. Dickson, Z. E. Gagnon, M. D. Coleman, P. Pechter, and J. G. Isebrands, 1993: Genetic variability in ozone response of trees: Indicators of sensitivity. *Agricoltura-Ricerca,* **15,** 16–17.

Koerber, M., R. Kaleel, L. Pocalujka, and L. Bruss, 1991: An overview of the Lake Michigan Ozone Study. Preprints, *Seventh Joint Conf. on Applications of Air Pollution Meteorology,* New Orleans, LA, Amer. Meteor. Soc., 260–263.

Lyons, W. A., C. J. Tremback, and R. A. Pielke, 1995: Applications of the Regional Atmospheric Modeling System (RAMS) to provide input to photochemical grid models for the Lake Michigan Ozone Study (LMOS). *J. Appl. Meteor.*, **34,** 1762–1786.

McKee, D. J., Ed.,1994: *Tropospheric Ozone: Human Health and Agricultural Impacts.* Lewis Publishers, 333 pp.

Mellor, G. L., and T. Yamada, 1982: Development of a turbulence closure model for geophysical fluid problems. *Rev. Geophys. Space Phys.*, **20,** 851–875.

NARSTO, 2001: NARSTO model comparison and evaluation study (MCES) update. *NARSTO News,* **5,** 3–13.

Philbrick, C. R., and Coauthors, 2002: Overview of the NARSTO-NE-OPS program. Preprints, *Fourth Conf. on Atmospheric Chemistry: Urban, Regional, and Global-Scale Impacts of Air Pollutants,* Orlando, FL, Amer. Meteor. Soc., 107–114.

Pielke, R. A., and Coauthors, 1992: A comprehensive meteorological modeling system—RAMS. *Meteor. Atmos. Phys.*, **49,** 69–91.

Reich, P. B., D. S. Ellsworth, B. D. Kloeppel, J. H. Fownes, and S. T. Gower, 1990: Vertical variation in canopy structure and CO_2 exchange of oak–maple forests: Influence of ozone, nitrogen, and other factors on simulated canopy carbon gain. *Tree Physiol.*, **7,** 329–345.

Rezabek, C. L., J. A. Morton, E. C. Mosher, A. J. Prey, and J. E. Cummings-Carlson, 1989: Regional effects of sulfur dioxide and ozone on eastern white pine (*Pinus strobus*) in eastern Wisconsin. *Plant Dis.*, **73,** 70–73.

Shafran, P. C., N. L. Seaman, and G. A. Gayno, 2000: Evaluation of numerical predictions of boundary layer structure during the Lake Michigan Ozone Study. *J. Appl. Meteor.*, **39,** 412–426.

Sillman, S., 1999: The relation between ozone, NO_x and hydrocarbons in urban and polluted rural environments. *Atmos. Environ.*, **33,** 1821–1845.

——, P. J. Samson, and J. M. Masters, 1993: Ozone production in urban plumes transported over water: Photochemical model and case studies in the northeastern and midwestern United States. *J. Geophys. Res.*, **98,** 12 687–12 699.

Tjoelker, M. G., J. C. Volin, J. Oleksyn, and P. B. Reich, 1995: Interaction of ozone pollution and light effects on photosynthesis in a forest canopy experiment. *Plant, Cell and Environ.*, **18,** 895–905.

Volin, J. C., M. G. Tjoelker, J. Oleksyn, and P. B. Reich, 1993: Light environment alters response to ozone stress in seedlings of *Acer saccharum Marsh* and hybrid *Populus L.* II. Diagnostic gas exchange and leaf chemistry. *New Phytol.*, **124,** 637–646.

Vukovich, F. M., 1979: A note on air quality in high pressure systems. *Atmos. Environ.*, **13,** 255–265.

——, 1995: Regional-scale boundary layer ozone variations in the eastern United States and their association with meteorological variations. *Atmos. Environ.*, 2259–2273.

Wang, D., D. F. Karnosky, and F. H. Bormann, 1986: Effects of ambient ozone on the productivity of *Populus tremuloides Michx.* grown under field conditions. *Can. J. For. Res.*, **16,** 47–55.

Zaveri, R. A., and L. K. Peters, 1999: A new lumped structure photochemical mechanism for large-scale applications. *J. Geophys. Res.*, **104,** 30 387–30 415.